1988PASJ...40..347F

Publ. Astron. Soc. Japan 40, 347–356 (1988)

Detection of Axisymmetric Filaments in the Filled-Center Supernova Remnant G21.5−0.9

Ernst Fürst,[1] Toshihiro Handa,[2] Koh-ichiro Morita,[2] Patricia Reich,[2] Wolfgang Reich,[1,2] and Yoshiaki Sofue[2,3]

[1]*Max-Planck-Institut für Radioastronomie, Auf dem Hügel 69, 5300 Bonn 1, F. R. G.*
[2]*Nobeyama Radio Observatory,* Minamimaki-mura, Minamisaku-gun, Nagano 384-13,*
[3]*Institute of Astronomy, Faculty of Science, The University of Tokyo, Mitaka, Tokyo 181*

(Received 1987 November 19; accepted 1988 February 1)

Abstract

High-resolution 22.3-GHz observations with the NRO Millimeter-wave Array of the filled-center supernova remnant G21.5−0.9 show a diffuse centrally peaked component and in addition axisymmetric filaments. The properties of the diffuse component and the morphology of the filaments suggest that they likely result from a two-sided collimated outflow of particles in precession from the central pulsar.

Key words: G21.5−0.9; Radio continuum emission; Supernova remnants.

1. Introduction

The supernova remnant (SNR) G21.5−0.9 is one of the brightest compact SNRs in our Galaxy. The high linear polarization, indicative of nonthermal characteristics, the flat radio spectrum, the centrally peaked morphology and its X-ray emission classify G21.5−0.9 as a filled-center type (Crab-like) or plerionic type SNR (Weiler 1983). Among the filled-center type SNRs it is the second most luminous source after the Crab Nebula in the radio and X-ray domain, i.e., the radio luminosity is about one sixth of the Crab Nebula and the X-ray luminosity about one fortieth for a minimal distance of 5.5 kpc taken from H I absorption data (Becker and Szymkowiak 1981; Davelaar et al. 1986). Although filled-center-type SNRs require the presence of a central source of energy (i.e. a pulsar), there is no observational evidence for such an object in G21.5−0.9 (Becker and Szymkowiak 1981), like in most other objects of this type.

* Nobeyama Radio Observatory, a branch of the National Astronomical Observatory is a facility open for general use by researchers in the field of astronomy, astrophysics, and astrochemistry.

© Astronomical Society of Japan • Provided by the NASA Astrophysics Data System

1988PASJ...40..347F

The magnetic field in G21.5−0.9 runs radially like in Cas A or other historical (young) shell-type SNRs (Becker and Szymkowiak 1981). Such a radial field is peculiar for a filled-center SNR, since SNRs of this type usually show a uniform magnetic structure, as it is the case for 3C 58, the Crab Nebula, and other objects (Weiler 1983), and may suggest that the conditions within G21.5−0.9 are different from other plerionic-type SNRs.

To clarify this we conducted high-frequency and high-resolution observations of G21.5−0.9 using the Nobeyama Millimeter-wave Array (NMA). The results of these observations are presented in section 3 and discussed in section 4 in terms of a high energy particle outflow from an assumed pulsar.

2. Observations and Data Reduction

The observations have been made on eight days between February and April 1987 using the NMA with eight different array configurations with 80 base lines. The details of the NMA have been described by Ishiguro et al. (1985). The center fre-

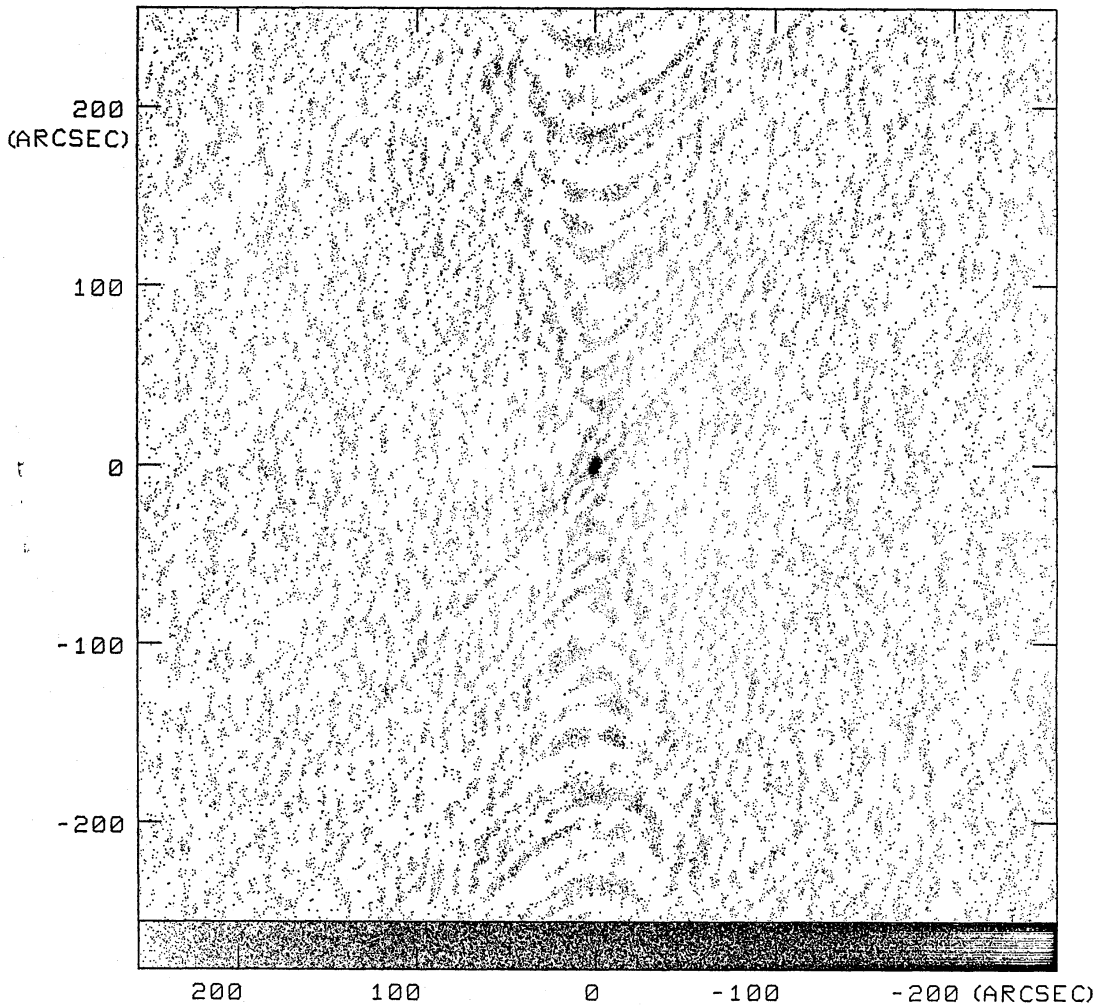

Fig. 1. Synthesized beam.

© Astronomical Society of Japan • Provided by the NASA Astrophysics Data System

1988PASJ...40..347F

Table 1. Parameters of the observations and data reduction.

Observations:	
Telescope	Nobeyama Millimeter-wave Array
Date	February 4–April 29, 1987
Array configurations	8
Number of base lines	80
Longest base line	~50 kilo wavelengths (=600 m)
Shortest base line	0.74 kilo wavelengths
Synthesized resolution	7″.3×4″.4 (at P. A. −15°.3)
Field center of G21.5−0.9	α (1950)=$18^h30^m47^s$, δ (1950)=−10°36′30″
Center frequency	22.3 GHz
Band width	250 MHz
Phase calibrator:	
NRAO 530	α (1950)=$18^h30^m13^s.534$, δ (1950)=−13°2′45″.78
	7 Jy during the observation period
Flux calibrator: 3C 286	2.55 Jy at 22.3 GHz
Data reduction:	
Software package	AIPS on FACOM M380S/VP50
Image processing procedure	CLEAN
R.m.s. noise	~1 mJy/beam

quency was 22.3 GHz, and the synthesized beam had a HPBW of 7″.3×4″.4 (figure 1). The frontends were cooled HEMT amplifiers (Kasuga et al. 1987) with a receiver temperature of about 300 K. As backend we used an analog correlator with a bandwidth of 250 MHz. The sampling time of each U–V data was 30 s. Since the observations were made by using right-handed circular polarization feeds at all antennae, only total intensity has been obtained.

The phase characteristic of the interferometer was checked by observing the compact source NRAO 530, which is located near G21.5−0.9, every 30 min during the observations. The source 3C 286 served as a primary intensity calibrator. The data reduction has been carried out using the AIPS package of the FACOM M380S and VP50 computers. We edited the visibility data, assumed a zero-spacing flux density of 6 Jy and made a map of the brightness distribution by a Fourier transformation. The CLEAN technique has been applied to the "dirty" map. Figure 1 shows the synthesized beam. The parameters of the observations, the calibration sources, and the data reduction are summarized in table 1. Finally the FITS-format of the maps was changed to apply the plot and analysis software, which we use for continuum observations with the NRO 45-m and Effelsberg 100-m telescopes.

3. Results

Figure 2 shows the 22.3-GHz map in its original resolution. Since the spectrum of G21.5−0.9 is known to be flat with α=0 ($S \propto \nu^{\alpha}$) for radio frequencies up to 32 GHz (Morsi and Reich 1987), the map very closely resembles the 5-GHz map of Becker and Szymkowiak (1981), which was observed with the VLA at a similar angular resolution. The source is slightly elliptical with a major axis length of ~1′.5 (at position angle ~35°) and an axial ratio of 0.8.

© Astronomical Society of Japan • Provided by the NASA Astrophysics Data System

1988PASJ...40..347F

To get a closer insight into the source properties we used a map smoothed to an 8″ circular beam and decomposed this map into a diffuse large-scale part and a small-scale source component by applying the "background filtering method" introduced by Sofue and Reich (1979). Using a circular 10″ filtering beam and running 12 iterations of the decomposition process we obtained the diffuse large-scale emission as shown in figure 3 and the remaining small-scale structures as shown in figure 4. To show the positional relation of the large-scale to the small-scale emission we show both components overlayed in figure 5.

The integration of the source components reveals that 85% of the total flux density is contained in the diffuse part and 15% in the small-scale emission structures. We performed an intensity integration of the diffuse emission in concentric rings starting from the source center. The result is shown in figure 6. The results for G21.5−0.9 from the present observations and the previous polarization and γ-ray observations by Becker and Szymkowiak (1981) are summarized in figure 7. The magnetic field direction shown in figure 7 was derived from the electric vector distribution corrected for a mean foreground Faraday rotation of -70 rad m^{-2}.

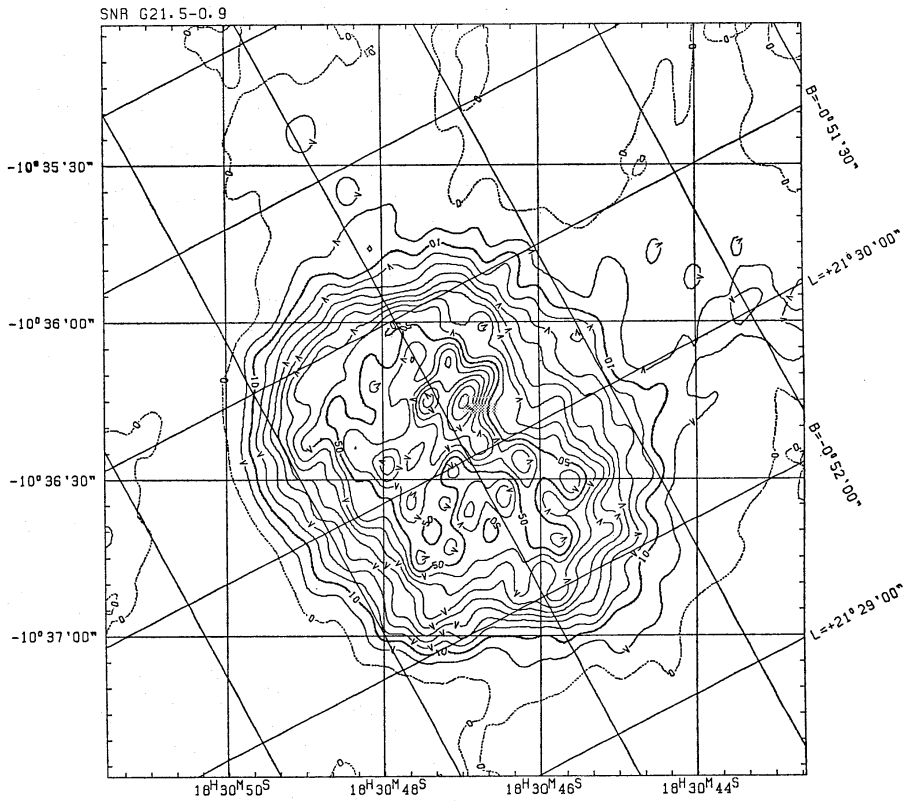

Fig. 2. Supernova remnant G21.5−0.9 at 22.3 GHz. The angular resolution is 7.″3 × 4.″4. Contours are shown in steps of 5 mJy/beam area. The center is at R. A. (1950) $=18^{h}30^{m}46^{s}.996$ and Decl. (1950) $=-10°36'30''.00$.

© Astronomical Society of Japan • Provided by the NASA Astrophysics Data System

1988PASJ...40..347F

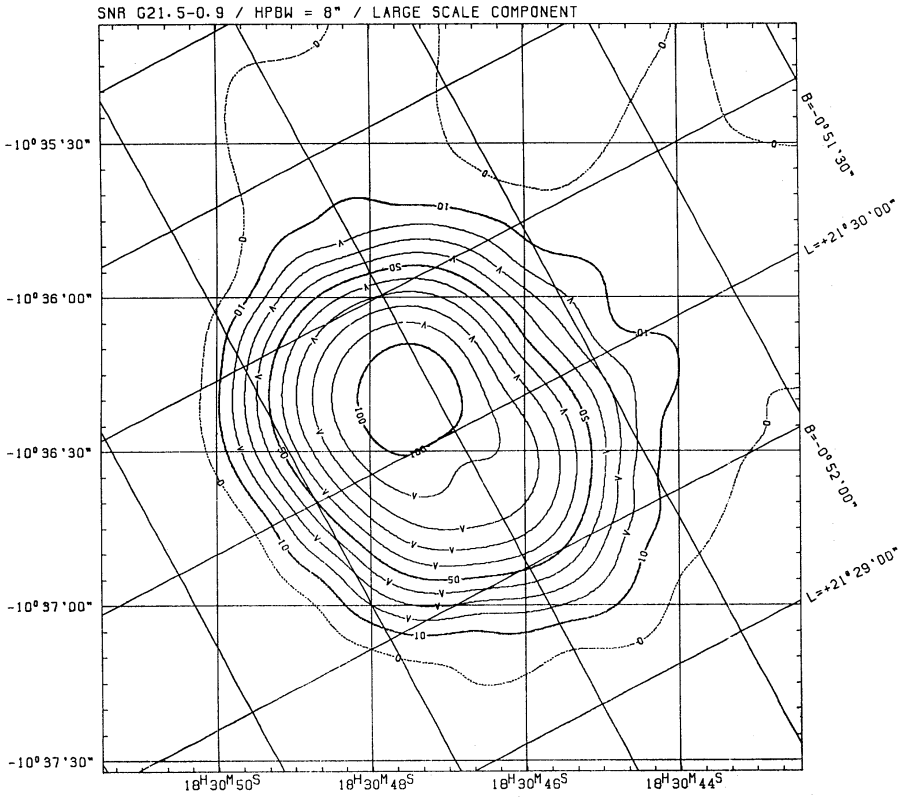

Fig. 3. Large-scale diffuse structure of G21.5−0.9 (see text). Contours are shown in steps of 10 mJy/beam area.

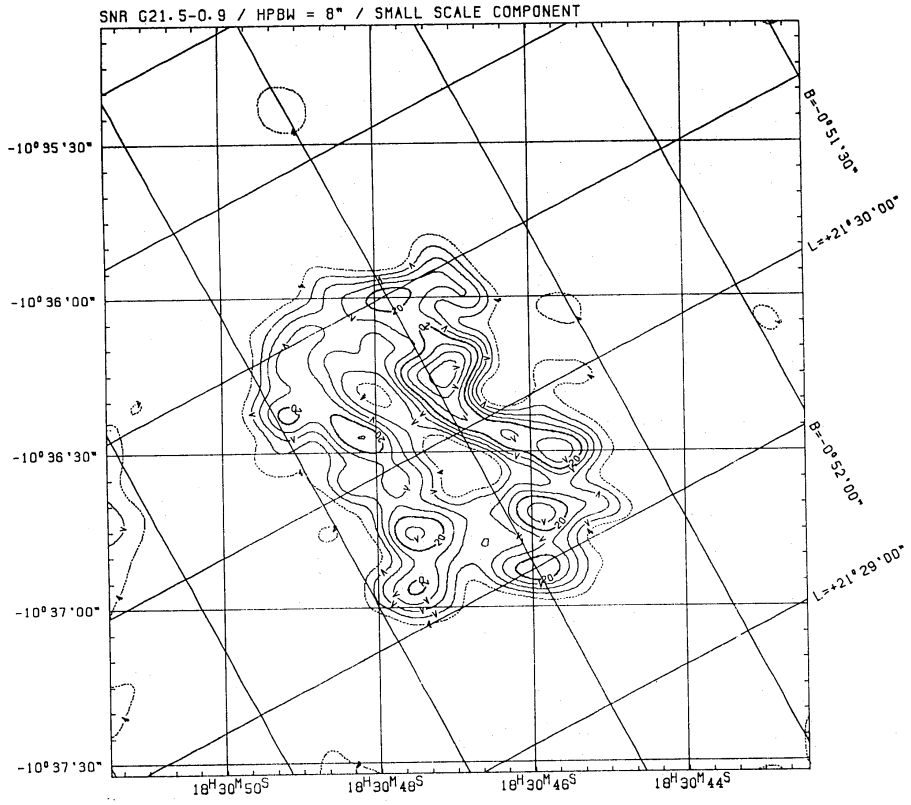

Fig. 4. Small-scale structures of G21.5−0.9 at 8″ angular resolution. Contours are shown for 4, 8, ···, 20, 25, ···, 35 mJy/beam area.

© Astronomical Society of Japan • Provided by the NASA Astrophysics Data System

1988PASJ...40..347F

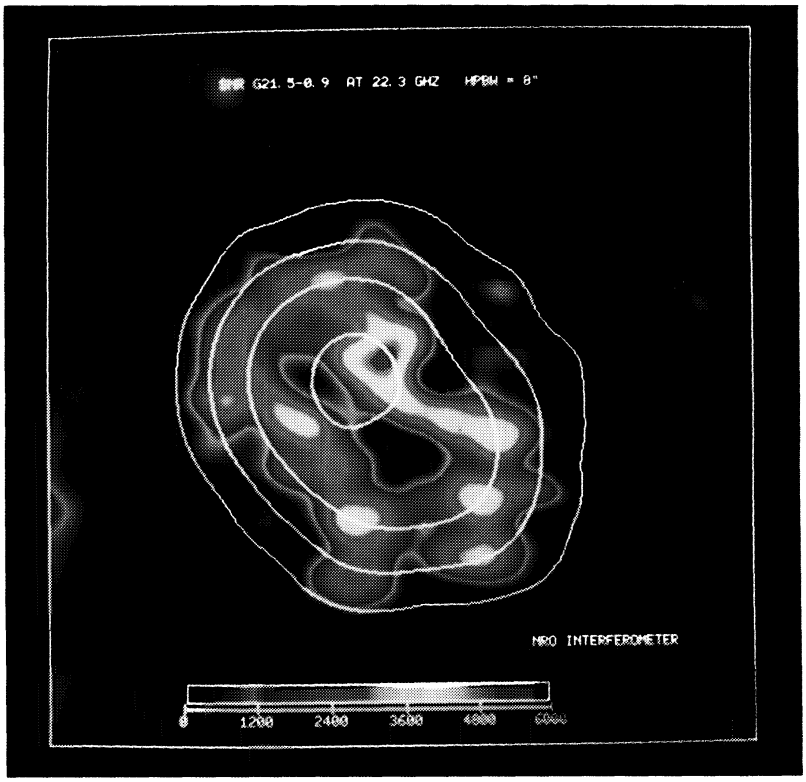

Fig. 5. Superposition of the small-scale emission (color coded) and the diffuse large-scale emission represented by contour lines. The angular resolution is 8″. The color bar scale is 10 mJy/beam area.

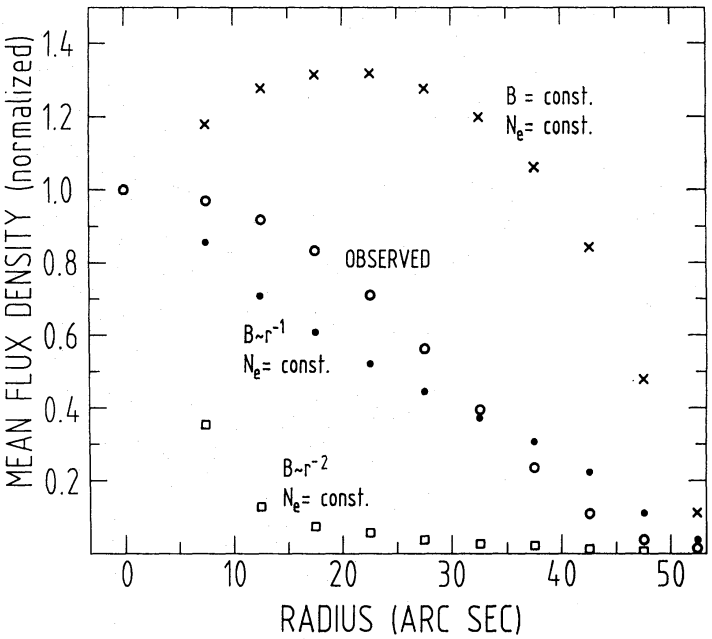

Fig. 6. The observed variation of synchrotron emission of the diffuse component of G21.5−0.9 (figure 4) with distance r from the center (open circles). Calculated profiles (for a ratio of radial-to-random magnetic field of 0.7) are shown for B=const., N_e=const. (crosses); for $B \propto r^{-1}$, N_e=const. (filled circles); and for $B \propto r^{-2}$, N_e=const. (squares).

© Astronomical Society of Japan • Provided by the NASA Astrophysics Data System

1988PASJ...40..347F

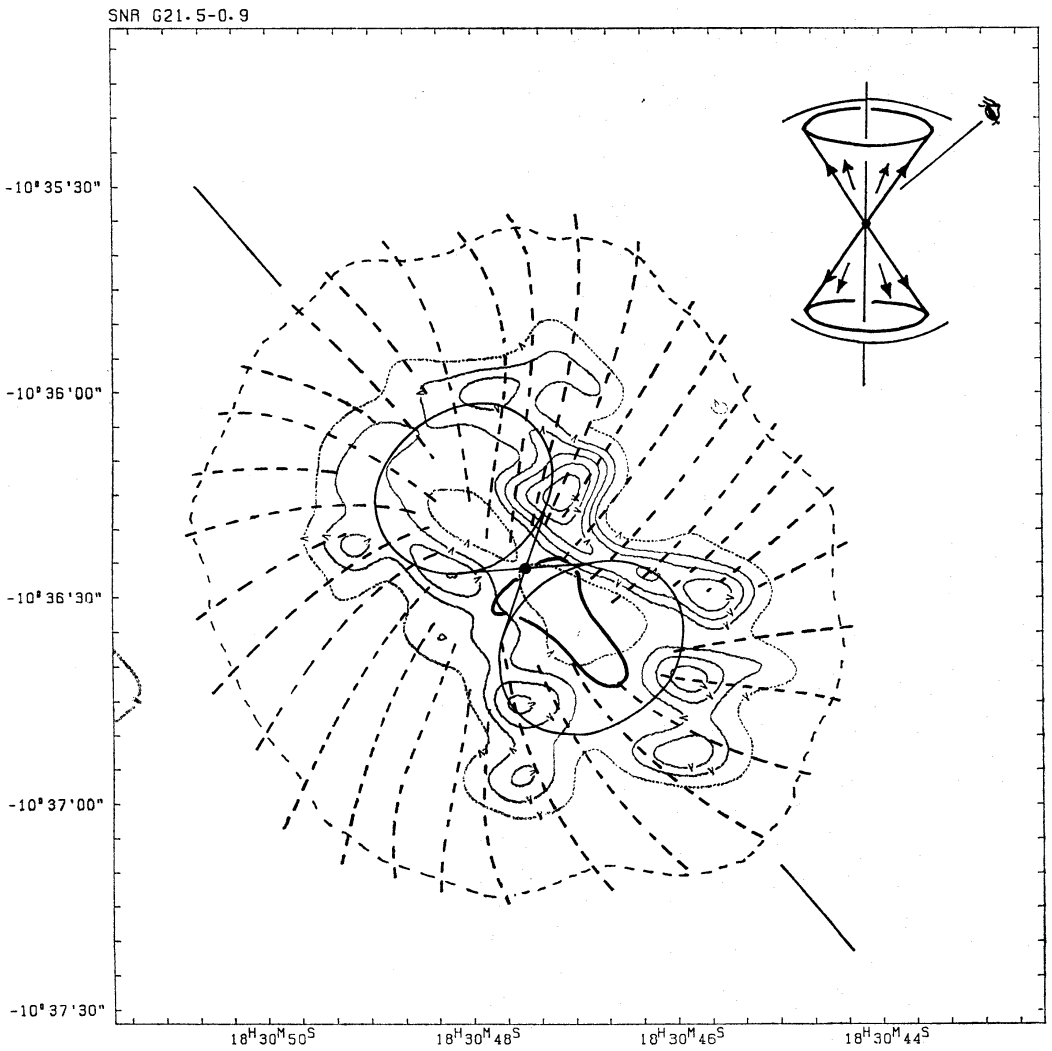

Fig. 7. Schematic view of G21.5−0.9. The small-scale radio emission (figure 5)[X] is shown in relation to the radial magnetic field direction and the maximum of the X-ray emission (black contour line) as observed by Becker and Szymkowiak (1981). Red contours at 7.5, 15, 20, ···, 35 mJy/beam area. The major axis is indicated by the straight line at P.A.=35° and a possible configuration for the pulsar jets is shown.

4. Discussion

Becker and Szymkowiak (1981) detected strong linear polarization of G21.5−0.9 at 5 GHz indicating an intrinsic radial magnetic field configuration as shown schematically in figure 7. The percentage polarization increases with radius and reaches values of $p=20\%$ to 30% near its boundary, while little polarization was found towards the center. This indicates its relation to the diffuse emission component (figure 3). The polarization intensity I_p peaks between the boundary and the center, where the polarization percentage is about 10%. This polarization characteristic is in agreement with the composition of the source magnetic field of a radial (B_{rad}) and a random (B_{ran}) component. If zero depolarization is assumed, the percentage polarization p of the detected synchrotron emission is $p=p_{max}B_{rad}^2/(B_{ran}^2+B_{rad}^2)$ (Burn 1966), where

© Astronomical Society of Japan • Provided by the NASA Astrophysics Data System

1988PASJ...40..347F

$p_{max}=(\alpha-1)/[\alpha-(5/3)]$ is the peak polarization of synchrotron emission of spectral index α (here $\alpha=0$, i.e., $p_{max}=60\%$). Near the boundary of G21.5−0.9, where $p=20\%$–30%, we obtain $B_{rad}/B_{ran}\sim 0.7$–1.0. Both components are of equal order.

The corresponding diffuse emission component (figures 3 and 6) shows a centrally peaked distribution. This reflects the dominant contribution from B_{ran} in the inner region of G21.5−0.9. (Because of geometrical effects, the contribution from B_{rad} is low.) The synchrotron emission integrated over the line of sight l is given by $\varepsilon_r l\sim\langle B^{\alpha+1}N_e\rangle l=\langle BN_e\rangle l$, where $\langle BN_e\rangle$ is the average product of the magnetic field perpendicular to the line of sight and the density of relativistic electrons. We estimated $\varepsilon_r l$ as a function of distance from the apparent source center assuming constant B and N_e ($B_{rad}/B_{ran}=0.7$), convolved to a HPBW of 8″, and estimated a profile to be compared with the observed profile in figure 6. Obviously, constant magnetic field and density N_e do not fit the observed profile. Conservation of magnetic flux leads to a decrease of the mean flux density much too rapidly: G21.5−0.9 defies the explanation in terms of an expanding synchrotron nebula. In figure 6 we also show a profile for $B\sim r^{-1}$, N_e=constant. Although it represents the data better, it is not satisfactory. The actual variation of B and N_e within G21.5−0.9 is more complicated and cannot be represented by a simple power law. However, a slight decrease of the product BN_e with radius is suggested.

The small-scale structures of G21.5−0.9, as displayed in figure 4, show high symmetry with respect to the minor and major axes of the SNR (see figure 7). The observed structures seem to consist of a superposition of a northern and a southern loop structure. The emission peaks are highly symmetric relative to the major axis except for the four emission blobs seen in the southern part of the SNR. The intensity is in general stronger on the western side. Since filled-centered SNRs are believed to be powered by a central pulsar, although these are not directly observed in most cases, it seems reasonable to assume that the symmetric emission structures are created by twin precessing jets or a collimated outflow of particles from the central pulsar. The overall geometrical structure of the filaments would place this pulsar near $\alpha_{50}=18^h45^m.5$, $\delta_{50}=-10°36'25''$ (see figure 7). It is, however, difficult to give details of the geometry of the double cone created by the precessing jets. The emission in the center is very low and may indicate that in this area the jets are directed close to the line of sight. For this case the magnetic field component perpendicular to the line of sight would be very low and consequently also the observed synchrotron emission. A schematic view for this case is shown in figure 7.

Such a scenario for pulsar–SNR associations has been sometimes proposed (e.g., Manchester and Durdin 1983; Fahlmann and Gregory 1983). However, convincing evidence is missing so far for the case of shell-type SNRs, because the enhanced SNR-shells, however, may result from some other mechanisms as well. Inside the SNR-shell these jets are invisible. If such jets exist inside filled centered SNRs they show up by interaction with the diffuse interior. The diffuse interior may be created independently beside the collimated outflow or it results from particles in the jets which are not strongly confined. In fact this seems to be the case for G21.5−0.9. In other plerionic-type SNRs like the Crab Nebula or 3C 58 the inner filamentary structures are more complex and less clearly ordered.

© Astronomical Society of Japan • Provided by the NASA Astrophysics Data System

1988PASJ...40..347F

A directed outflow of particles in G21.5−0.9 may account for the slow decrease of BN_e with r from the center as found for the diffuse emission component. However, some details of the southern and northern cones are different, e.g., the southern maxima are more distant from the minor axis than the northern maxima. While this may simply reflect a different magnetic field strength or orientation of the magnetic field direction relative to the line of sight, it may also reflect some change of the outflow center with time.

By comparing our radio maps with the X-ray emission map shown by Becker and Szymkowiak (1981) we note that the region showing maximum X-ray emission is located southwest of the center of the small-scale radio emission (see figure 7). It nicely coincides with the minimum of the radio emission. This in fact suggests different release processes for the particles showing up in the radio and X-ray ranges. From luminosity considerations for plerionic-type SNRs it was already concluded that their particle spectra must be different (e.g., Davelaar et al., 1986).

The X-ray spectrum of G21.5−0.9 was recently observed with EXOSAT by Davelaar et al. (1986) and was found to be $\alpha = -0.59$ to -0.84 ($S \propto \nu^{\alpha}$), which implies a harder energy spectrum in comparison with other plerionic-type SNRs. Since the lifetime for the X-ray radiating particles is about $\sim 1/1000$ that of particles radiating in the radio range, one may assume that the pulsar is located at present close or within the X-ray emission maximum. Since the peak of the diffuse synchrotron radiation is located slightly north of the minor axis (see figures 3 and 5), we may consider some movement of the pulsar along the major axis from north to south (roughly along galactic latitude b) to account for these asymmetries between the diffuse radio and X-ray emission and it may also explain the north-south asymmetry of the small-scale emission maxima.

The distance to G21.5−0.9 was determined by recent H I-absorption measurements with the VLA by Davelaar et al. (1986) to be within 5.5 kpc and 9.3 kpc. This gives a maximum extent of G21.5−0.9 along its major axis of 2.4 pc or 4 pc respectively. The peaks of the diffuse radio and the X-ray emission are in any case less than ~ 0.6 pc apart. The age of G21.5−0.9 is unknown. From its very low luminosity compared to the Crab Nebula despite its smaller size, one may conclude that G21.5−0.9 is the elder object. If we assume an age of ~ 5000 yr, we obtain a projected pulsar velocity of less than ~ 120 km s^{-1} depending on its distance. This value is quite close to the mean component for pulsar velocities perpendicular to the galactic plane as given by Lyne (1981).

5. Conclusion

Our high-resolution measurements of G21.5−0.9 reveal a centrally peaked diffuse emission and a symmetrical double cone structure, which may be interpreted as the signature of precessing jets from an assumed central pulsar. Particles radiating in the radio range may be transferred via these jets into the diffuse emission region. This may explain the slow decrease of the radio emissivity with the distance from the SNR center, which is inconsistent with a constant isotropic particle outflow. The maximum of the X-ray emission is located within a radio minimum. Both types of emission

© Astronomical Society of Japan • Provided by the NASA Astrophysics Data System

1988PASJ...40..347F

originate from different particle spectra and seem to be released from the pulsar in a different way. The north-south asymmetry between the X-ray and radio maxima may be explained by a pulsar movement with a transverse velocity as found for the average of pulsars, if the age of the SNR is not much smaller than ~ 5000 yr.

P. R. and W. R. are indebted to the Japan Society for the Promotion of Science for financial support. We thank the staff of NRO for their extensive help in the observations and reductions, and in particular, Professor M. Ishiguro for his invaluable discussions. This work was supported in part by the Ministry of Education, Science, and Culture under Grant No. 61460009 (Y.S.).

References

Becker, R. H., and Szymkowiak, A. E. 1981, *Astrophys. J. Letters*, **248**, L23.

Burn, B. J. 1966, *Monthly Notices Roy. Astron. Soc.*, **133**, 67.

Davelaar, J., Smith, A., and Becker, R. H. 1986, *Astrophys. J. Letters*, **300**, L59.

Fahlmann, G. G., and Gregory, P. C. 1983, in *Supernova Remnants and Their X-Ray Emission, IAU Symp. No. 101*, ed. J. Danziger and P. Gorenstein (D. Reidel Publishing Company, Dordrecht), p. 445.

Ishiguro, M., Morita, K.-I., Kasuga, T., Kanzawa, T., Iwashita, H., Chikada, Y., Inatani, J., Suzuki, H., Handa, K., Takahasi, T., Tanaka, H., Kobayashi, H., and Kawabe, R. 1985, in *Millimeter and Submillimeter Wave Radio Astronomy, URSI Symp.*, ed. J. Gómez-González (Imprenta Ntra. Sra. de las Angustias, Granada), p. 75.

Kasuga, T., Kawabe, R., Ishiguro, M., Yamada, K., Kurihara, H., Niori, M., and Hirachi, Y. 1987, *Rev. Sci. Instrum.*, **58**, 379.

Lyne, A. G. 1981, in *Pulsars, IAU Symp. No. 95*, ed. W. Sieber and R. Wielebinski (D. Reidel Publishing Company, Dordrecht), p. 423.

Manchester, R. N., and Durdin, J. M. 1983, in *Supernova Remnants and Their X-Ray Emission, IAU Symp. No. 101*, ed. J. Danziger and P. Gorenstein (D. Reidel Publishing Company, Dordrecht), p. 421.

Morsi, H. W., and Reich, W. 1987, *Astron. Astrophys. Suppl.*, **69**, 533.

Sofue, Y., and Reich, W. 1979, *Astron. Astrophys. Suppl.*, **38**, 251.

Weiler, K. W. 1983, in *Supernova Remnants and Their X-Ray Emission, IAU Symp. No. 101*, ed. J. Danziger and P. Gorenstein (D. Reidel Publishing Company, Dordrecht), p. 299.

© Astronomical Society of Japan • Provided by the NASA Astrophysics Data System